Int. J. Electrochem. Sci., 8 **(2013)** 4827 - 4838

International Journal of
ELECTROCHEMICAL
SCIENCE
www.electrochemsci.org

Microfluidic Direct Methanol Fuel Cell with Ladder-Shaped Microchannel for Decreased Methanol Crossover

Weiwei Huo[1,2], *Yi Zhou*[1], *Haifeng Zhang*[1], *Zhiqing Zou*[1,*] *Hui Yang*[1,*]

[1] Shanghai Institute of Microsystem and Information Technology, and Shanghai Advanced Research Institute, Chinese Academy of Sciences (CAS), Shanghai, 201210, P. R. China
[2] Graduate School of the CAS, Beijing 100039, P. R. China
[*]E-mail: zouzq@sari.ac.cn; yangh@sari.ac.cn

Received: 10 January 2013 / *Accepted:* 27 February 2013 / *Published:* 1 April 2013

In this work, the design and fabrication of a planar, glass- polydimethylsiloxane based microfluidic direct methanol fuel cell with ladder-shaped microchannel are presented. The fuel cell operates in an acidic electrolyte and with methanol and H_2O_2 as fuel and oxidant, respectively. The novel ladder-shaped microchannel leads to a significant improvement in minimizing reactant crossover, which could keep the diffusive interface away from the opposite electrode. A three-dimensional diffusion-convection model is developed to investigate the behavior of the mixing zone and to extract appropriate cell parameters and operation conditions. The fluorescence experiments show that the ladder-shaped microchannel structure leads to a decrease in width of the mixing zone. The proof-of-concept microfluidic direct methanol fuel cell with ladder-shaped microchannel is able to reach a maximum power density of 12.24 mW cm^{-2} at a flow rate of 0.5mL min^{-1}, which is ca. 35.3% higher than that of a normal shaped microfluidic direct methanol fuel cell.

Keywords: Microfluidic direct methanol fuel cell, Laminar flow, Ladder-shaped microchannel, Fluid crossover

1. INTRODUCTION

With advances in cellular phones, laptop computers and electronic devices, direct methanol fuel cells (DMFCs) have recently emerged as a new power source because of their high energy density to replace the traditional power sources, such as rechargeable Li-ion batteries [1]. Of various fuel cell systems, the microfluidic fuel cells have been recognized as one of the most promising candidates for small-scale portable power generation [2-5]. A microfluidic fuel cell is characterized by its fluid delivery and removal, reaction sites and electrode structures all confined to a microfluidic channel. This special kind of cells typically operates in a co-laminar flow configuration without a physical

barrier to separate the anode and the cathode. Due to the laminar nature of the flow in microstructures, the crossover between fuel and oxidant streams can be effectively suppressed. However, for practical applications, several issues need to be addressed. The most prominent constraint is its low power density due to the low utilization of dissolved oxygen and the slow kinetics of both anode and cathode.

Since the performance of a microfluidic fuel cell is mainly determined by the diffusion across the interface between the liquid streams, it is important to design a novel microchannel to prevent the crossover of the fuel and oxidant. Ferrigo et al [6] first proposed a vanadium redox membraneless fuel cell using a Y-shaped millimeter-scale channel. Such a design exploits the laminar flow that occurs in liquids flowing at low Reynolds number (Re) to eliminate convective mixing of fuel and oxidant. Choban et al [7] also designed a microfluidic fuel cell using a Y-shaped channel. The fuel used in their work is formic acid and the oxidant dissolved oxygen. They found that the cell performance is considerably reduced by the transport of reactants through the concentration boundary layer adjacent to the electrodes and the low concentration of oxygen in cathode stream. Ned Djilali et al [8] gave a numerical analysis of a microfluidic DMFC. Their numerical simulations showed that both microchannel and electrode geometric size are quite important for the improvement in fuel cell performance. From the numerical simulation, an extended taper-shaped electrode structure was proposed. Such a new microfluidic fuel cell with the taper-shaped electrode demonstrates that the fuel utilization is over 50%. Chang et al [9] also conducted a numerical analysis at a given flow rate and a fixed channel cross-sectional area. Their results showed that the geometric parameters of the channel played an important role in cell performance. For a constant cross sectional area, a larger aspect ratio would be preferred. Kenis et al [10] fabricated a bridge-shaped microchannel to minimize reactant crossover and to isolate the corresponding mixing zone from the electrode areas. Such a structure not only enables an efficient proton transport, but also increases the reactive area, thus improving the fuel utilization.

Generally, the oxidant used in a microfluidic DMFC is the dissolved oxygen in the solution. However, the very low O_2 concentration in the solution leads to a low power density. To address this problem, other oxidants such as hydrogen peroxide (H_2O_2) [11-12] and potassium permanganate ($KMnO_4$) [7, 13-14] with high concentration have been used to improve the cathode performance of the microfluidic DMFC.

In this work, we report the design, simulation and fabrication of a new ladder-shaped microfluidic DMFC using methanol and H_2O_2 as fuel and oxidant, respectively. The ladder-shaped microchannel confines the diffusive liquid-liquid interface to regions away from the opposite electrodes. Based on our experimental data, the maximum power density of our proof-of-concept microfluidic DMFC may reach 12.24 mW cm^{-2} at ambient temperature.

2. THEORETICAL MODEL AND CONSIDERATION

2.1. Theoretical consideration

The microfluidic fuel cell in this work uses methanol as the fuel and H_2O_2 as the oxidant. The fuel and oxidant could be separated by a limited liquid-liquid interface as well as the fluid, showing

laminar flow character when the characteristic size of microchannel is decreased to micrometer scale. The Peclet number, which provides an indication of the relative importance of diffusion and convection, is an important parameter for laminar. The Peclet number is defined as:

$$Pe = U_y H / D \quad (1)$$

where U_y is the average flow velocity, H is a characteristic length of the system perpendicular to the direction of the flow and D is the diffusion coefficient of the particle or molecule of interest, which has a positive correlation with the width of channel. When the transverse diffusion is much slower than the convection, the mixing zone may be restricted to a thin interfacial width in the center of the channel. Because of cross diffusion of the fuel and the oxidant, the liquid-liquid interface evolves into a mixing zone which gradually expands in width along the fluid channel. The fuel crossover would result in the degradation of the fuel cell performance. The calculated width of the diffusion mixing region is in agreement with the theoretically predicted and experimentally trend represented by the form [10, 15]:

$$\delta_x \propto \left(DHl/U \right)^{1/3} \quad (2)$$

where δ_x is the diffusion mixing region and l is the length of mixing zone for a normal microchannel.

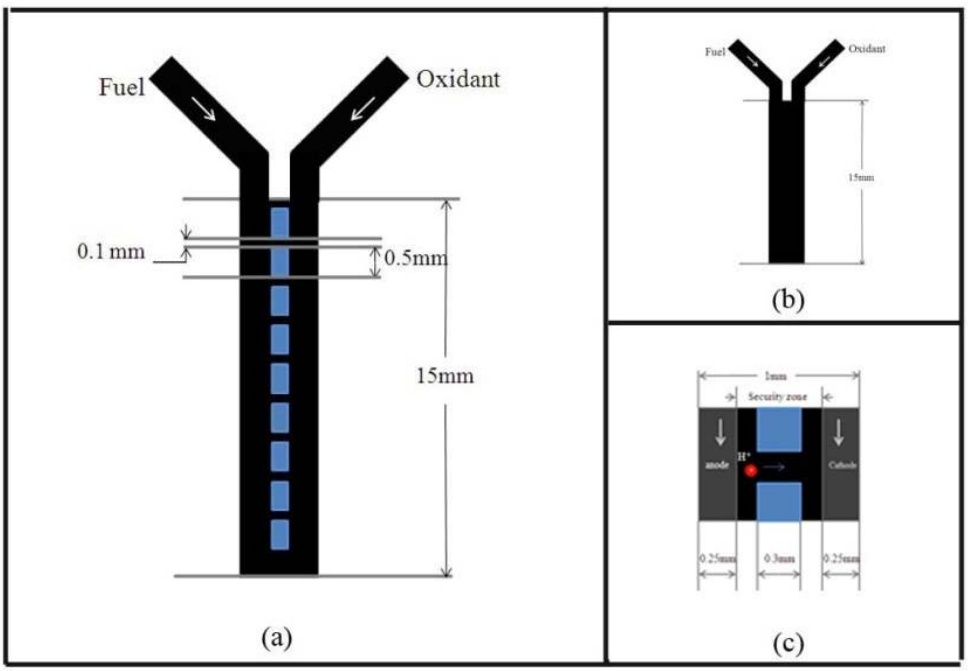

Figure 1. Schematic top views of the ladder-shaped (a. c) and normal shaped (b) microchannel structure and geometric parameters employed in the simulation.

Fig. 1a illustrates the top views of the novel microchannel structure. There is a ladder shaped wall in the microchannel to separate the anode from the cathode, but there are many gaps in the wall, through which the protons diffuse freely but in which diffusion of the reactants is limited. For normal shaped microchannel, two electrodes are integrated side by side at the bottom of a single microchannel (Fig. 1b), and the parameter "*l*" is equal to the length of the fluid flows downstream. While for a ladder-shaped microchannel, the parameter "*l*" is the effective length of the widths of the gaps, which is much smaller than its actual length. Thus, the diffusion transverse to the direction of flow could be minimized by decreasing effective *l.* It could be beneficial to minimize fuel-to-oxidant diffusive contact.

2.2. Governing equations and mixing-zone model

Typically, the dimension of main microchannel is 150 μm in depth, 1000 μm in width and 15 mm in length. The anode and cathode are located side by side on the bottom of the microchannel with a width of 250 μm and length of 10 mm. Between the electrodes, there is a special zone without catalyst in order to reduce the effects of fuel crossover on the electrodes, which is considered to be a "security zone" (Fig. 1c). The model was implemented in Fluent. Fluent is a branch of fluid mechanics that uses numerical methods and algorithms to solve and analyze problems that involve fluid flows. According to the continuum and laminar nature of the liquids in microchannels [16], some assumptions should be made to obtain a simplified model: (1) the density of the fluid and the velocity are constant; (2) the body forces such as the fluid weight are dominated by surface forces such as viscous shear stress. Applying mass and momentum conservation, the velocity fields could be described by the Navier – Stokes and continuity equations:

$$\rho\left(\frac{\partial\vec{u}}{\partial t}+\vec{u}\cdot\nabla\vec{u}\right)=-\nabla p+\mu\nabla^2\vec{u}+\vec{f} \qquad (3)$$

In these equations, *u* and *p* represent the velocity and pressure, respectively. ρ and μ denote the density and viscosity, $\vec{f}$ summarizes the body forces per unit volume. At very low Reynolds numbers, the non-linear convective terms can be neglected, resulting in linear and predictable Stokes flow:

$$\rho\frac{\partial\vec{u}}{\partial t}=-\nabla p+\mu\nabla^2\vec{u}+\vec{f} \qquad (4)$$

Furthermore, mass conservation for fluid flow obeys the continuity equation and the incompressibility condition with the assumptions:

$$\frac{\partial\rho}{\partial t}+\nabla\cdot\left(\rho\vec{u}\right)=0 \qquad (5)$$

$$\nabla \cdot \vec{u} = 0 \qquad (6)$$

3. EXPERIMENTAL PART

3.1. Fabrication of the microfluidic fuel cells

The microfabrication process of the microfluidic DMFC includes the following steps: development of patterned electrodes and deposition of the electrocatalysts on a glass substrate; developing and replicating polydimethylsiloxane (PDMS) chip with microchannels by a UV-LIGA (i.e., Lithographie, Galanoformung, Abformung: in English, Lithography, Electroplating, and Molding) process; integrating the microchannels with the electrodes by PDMS-glass bonding.

The electrode-patterns were developed on a substrate of 0.5 mm thick PYREX glass wafer by a photolithographic process as shown schematically in Fig. 2a.

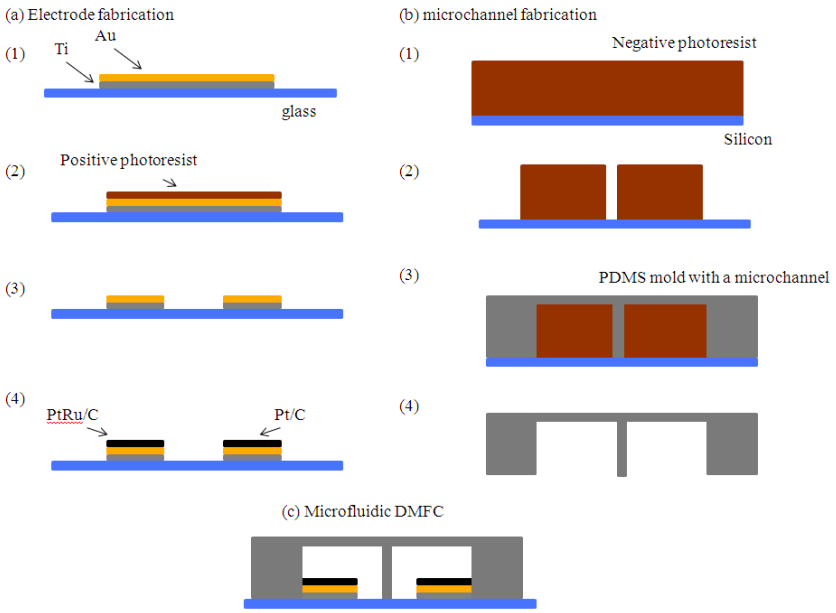

Figure 2. Typical microfabrication process for the microfluidic fuel cell (a) Electrode fabrication: (1) successive deposition of 20 nm Ti and 100 nm Au as seed layer. (2) coating of the positive photoresist for photolithography. (3) patterning the electrodes. (4) deposition of Pt-based catalyst via EPD. (b) Microchannel fabrication: (1) spraying the SU-8 negative photoresist on a silicon wafer. (2) patterning the reverse microchannel via lithography. (3) covering the negative channel with PDMS. (4) curing the PDMS for getting a microchannel. (c) integrating the microchannels with the electrodes by PDMS-glass bonding (sectional view).

Briefly, electro-conductive layers of 20 nm of Ti and 100 nm of Au were deposited on the glass wafer via sputtering [17]. Then, the glass wafer was spin-coated with positive photoresist and exposed to photolithography. After developing, the exposed metal layers were etched by corresponding etching solutions. Finally, the residue photoresist was removed by acetone and the wafer was cleaned by rinsing with abundant ethanol and ultrapure water.

The electrocatalyst was deposited by electrophoretic deposition (EPD) process. The solution was prepared by mixing 50 mg of carbon-supported Pt-Ru catalyst (Pt 40wt.%, Ru 20wt.%, HiSpec 10000) or carbon-supported Pt catalyst (Pt 60wt.%, HiSpec9000), 125 mg of Nafion solution (5%, Dupont) with 400 mL of isopropyl alcohol. Then, the catalysts were electrophoretically deposited onto the electrode by applying a constant voltage of 10 V and a distance of 10 mm between the counter electrode and working electrode. The typical deposition time was 1 min. Subsequently, the electrode deposited with the catalyst was rinsed with ultrapure water and isopropyl alcohol. Finally, the chips were dried at 60 ^{o}C under vacuum for 1 h, in order to increase the adhesion.

A microfluidic fuel cell consisting of a ladder-shaped channel with electrodes on sidewalls of the main channel was fabricated using reported typical procedures (Fig. 2b.) [18-19]. The reverse microchannel was fabricated by a thick photoresist (SU-8 series, MicroChem) via a soft lithography technique. The mold was then replicated with PDMS (polydimethylsiloxane, Sylgard 184, Dow Corning Inc., Midland, MI) to produce a microfluidic channel [20]. After depositing the appropriate catalyst on the electrode, the PDMS chip with a microchannel was inversely bonded to the patterned glass substrate by plasma treatment. Access holes for inlets and outlets were punched from the top part of the microchannel before sealing. The final structure of the DMFC is shown schematically in Fig. 2c. For a comparison, a microfluidic DMFC with normal microchannel was prepared following the same procedure and shown in Fig. 1b.

3.2. Fluorescence measurement and microfluidic fuel cell testing setup

In order to maintain co-laminar flow, the fuel and oxidant solutions were pumped with a uniform fluid velocity generated by a pump (KD Scientific, KDS 200). The fluorescence measurement was first conducted prior to the electrochemical test [21]. In this study, solutions for fluorescence measurements were prepared by mixing the Rhodamine and ultrapure water in a volume ratio of 1:10.

The electrochemical performance of the microfluidic fuel cell was investigated by steady-state polarization using fuel cell testing system (ARBIN). The fuel cell was fed with a mixture of 2 M CH_3OH + 0.5 M H_2SO_4 as anolyte and a mixture of 2 M H_2O_2 + 0.5 M H_2SO_4 as catholyte. The flow velocity was 0.5 mL min^{-1} for both fuel and oxidant liquids and the channel cross section was about 0.1 mm^2. All the electrochemical measurements were carried out at a temperature of ca. 25 ^{o}C.

4. RESULTS AND DISCUSSION

4.1. Simulation and fluorescence analysis

Fig. 3 illustrates the diffusive behavior of methanol at the fuel flow downstream with the variation of fluid velocity by simulation. Fig. 3(a) shows the concentration profile when the cell is fueled with 2 M methanol at a flow rate of 0.5 mL min^{-1}. Fig. 3(b) is the methanol concentration profiles on the *X-Z* plane at three locations downstream from the active cell entrance (0.6, 4.2 and 10.2

mm). It can be seen that the width of the mixing zone gradually expands as the flow runs to the exit, but is still confined to within the channel. According to equation 2, there is a positive correlation between the mixing zone width and length of mixing zone for a normal microchannel. Our simulation results are in good agreement with the previous experimental studies [10, 15].

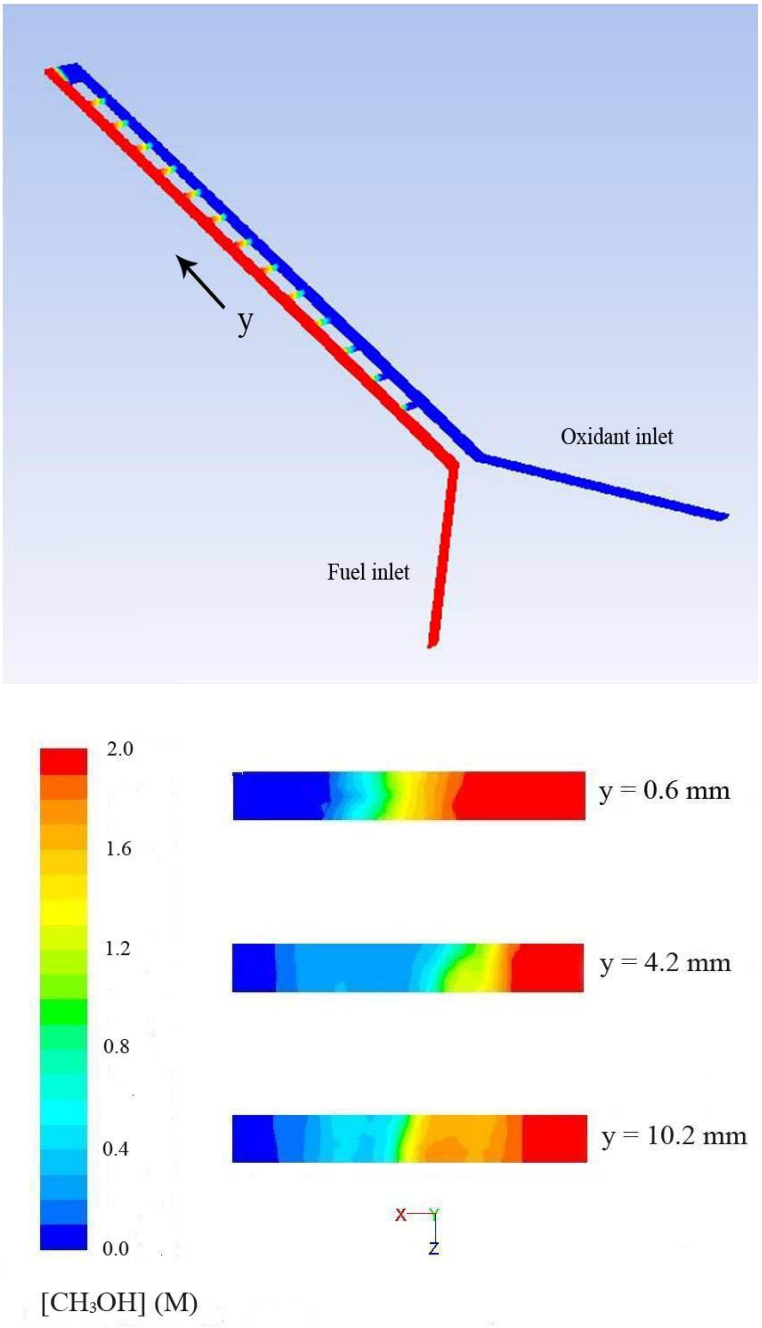

Figure 3. Methanol concentration profiles for a ladder-shape microchannel when fed with 2 M CH_3OH at a flow rate of 0.5 mL min^{-1}:(a) 3D flow domain;(b) 2D captured with X-Z planes located at three different locations from the channel entrance.

According to equation 1, the mixing zone width may be controlled by flow velocity. Fig. 4a depicts the fuel concentration profile at the location of 4.2 mm from the cross point of the normal

shaped microchannel. The concentration gradients are simulated at different flow rates. The width of mixing zone becomes narrower with an increase in flow rate, which fits well with the empirical equation (Eq. 1). For the microfluidic DMFC, the mixing zone should always be narrower than the "security zone".

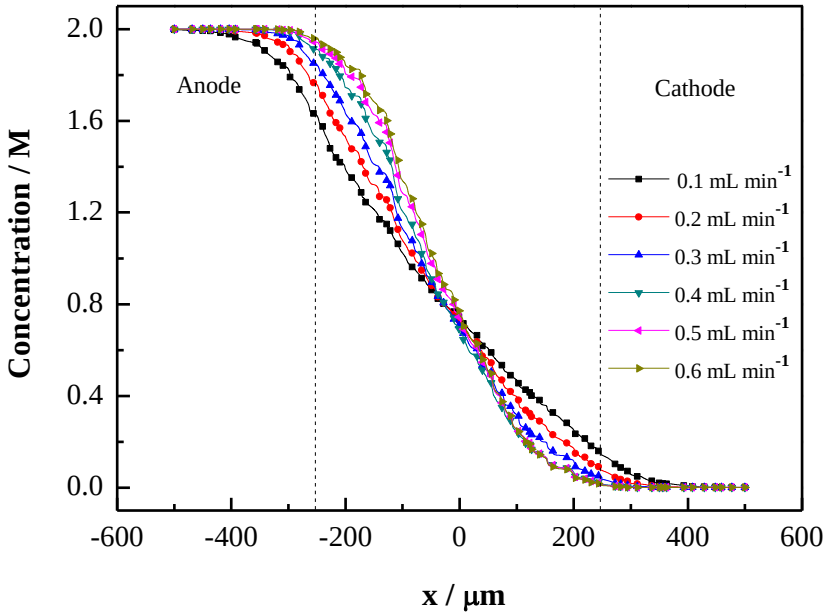

(a)

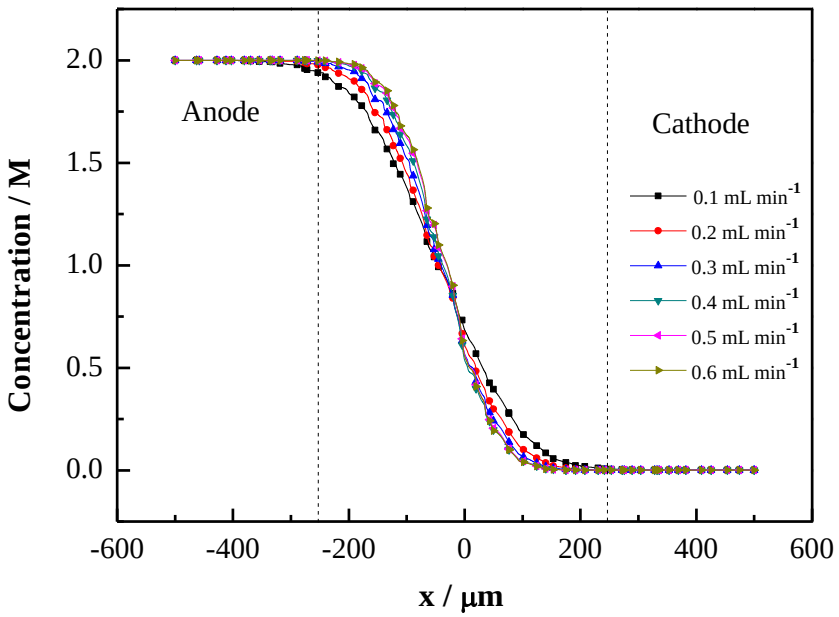

(b)

Figure 4. Methanol concentration gradients at a location of 4.2 mm from the active cell entrance at the different flow rates with normal shaped (a) and ladder-shaped (b) microchannels.

Fig. 4b shows a similar mixing tendency for ladder-shaped microchannel. A comparison of Fig. 4a and Fig. 4b suggests that the concentration gradients with a ladder-shaped microchannel are more convergent than those with a normal shaped microchannel, indicating that the fuel crossover is decreased by using the ladder-shaped microchannel, effectively avoiding the "mixed potential" at the cathode.

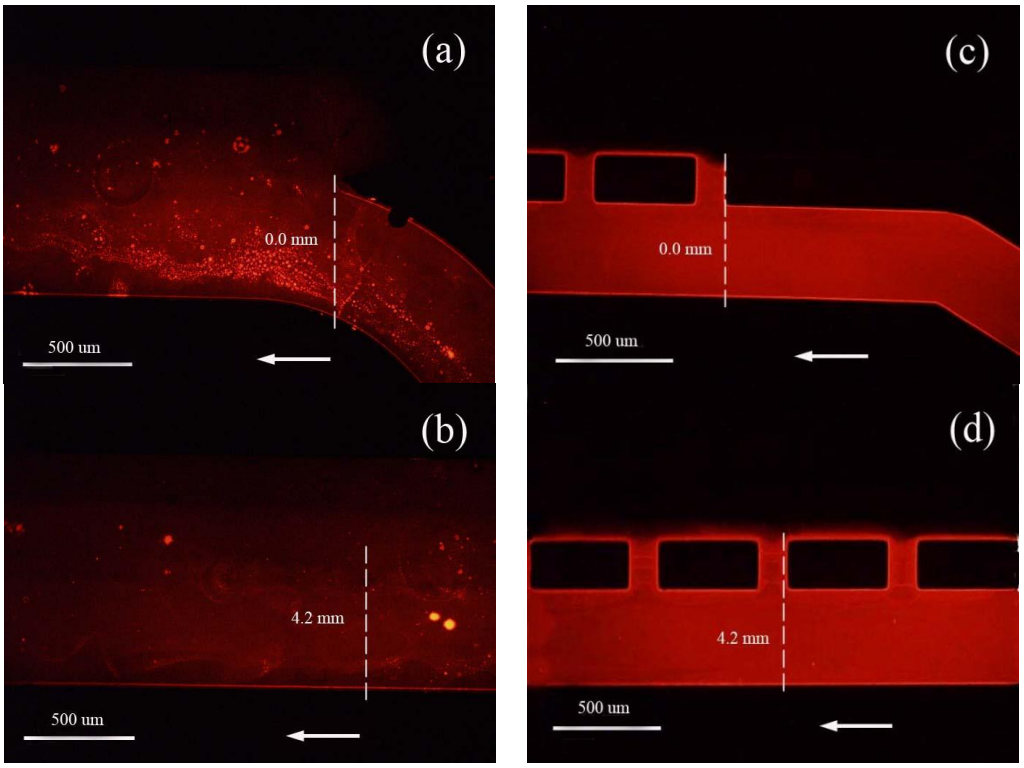

Figure 5. Fluorescence results for normal shaped microchannel (a. b) and ladder-shaped microchannel (c. d) at different locations.

The fluorescence results for the two microchannels at different locations are shown in Fig. 5. By comparing the two groups of results, it is clear that the diffusion phenomenon is more pronounced in a normal shaped microchannel than a ladder-shaped microchannel. It is however, difficult to make a quantitative evaluation between the theoretical prediction and experimental results. Nevertheless, the cell performances in both cases are in fairly good agreement.

4.2. Performance comparison of the microfluidic DMFCs

The performance of the microfluidic DMFC with ladder-shaped microchannel at flow rate variation from 0.1 to 0.6 mL min^{-1} is given in Fig. 6. Polarization curves indicate the open cell voltage (OCV) of the DMFC increases from 0.84, 0.89, 0.97 to 0.96 V while the flow rate is varied from 0.1, 0.3, 0.5 to 0.6 mL min^{-1}, respectively. The change in OCV is attributed to the decreased reactant crossover at higher flow rates. These data are in good agreement with our simulated results. The

maximum power densities of such microfluidic DMFCs are 6.99, 8.88, 12.24, 12.06 mWcm^{-2} at the flow rate of 0.1, 0.3, 0.5 and 0.6 mL min^{-1}, respectively.

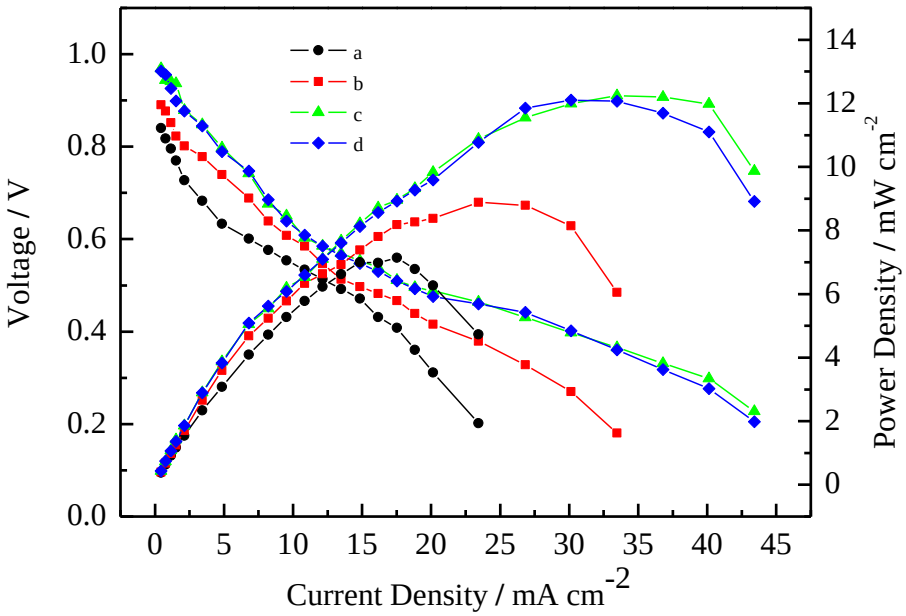

Figure 6. Performance comparison of the microfluidic DMFCs with ladder-shaped microchannel at flow rate of 0.1 mL min^{-1}(a), 0.2 mL min^{-1}(b), 0.5 mL min^{-1}(c) and 0.6 mL min^{-1}(d) at 25 ^{o}C.

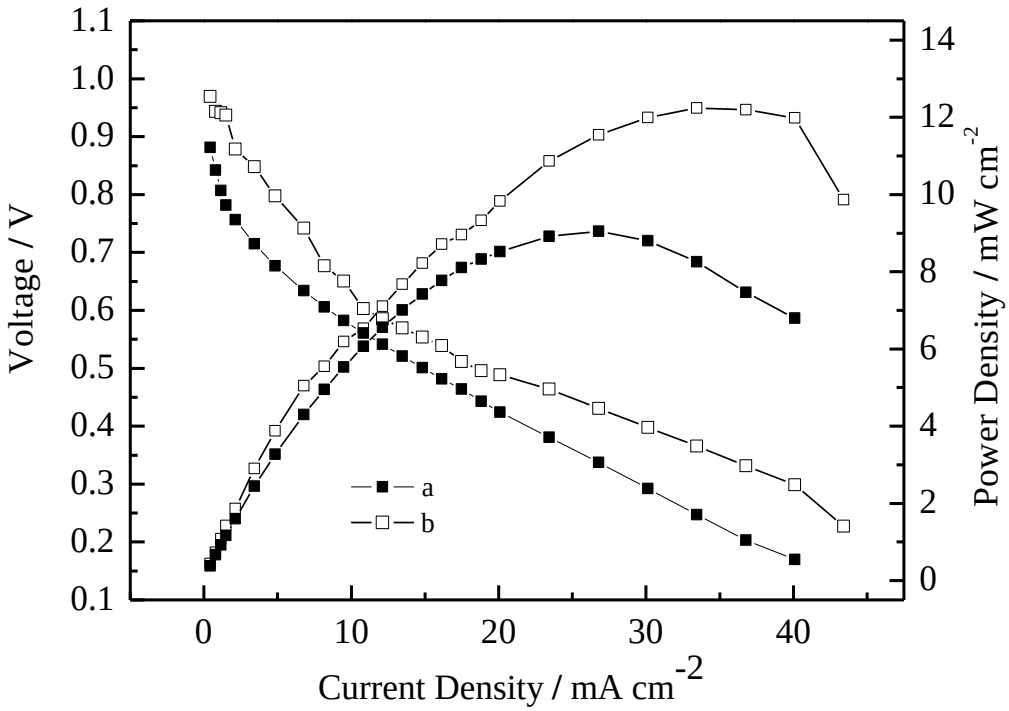

Figure 7. Polarization curves of the microfluidic DMFCs with normal shaped microchannel (a) and ladder-shaped microchannel (b) at a temperature of 25 ^{o}C and a flow rate of 0.5mL min^{-1}.

The increased average velocity results in a thinner mixing zone, as shown by simulation. In addition, higher flow rate will be helpful to better supply reactants and remove reaction products. However, the power density does not improve for the flow rate higher than 0.5mL min^{-1}, because the reactants keep a dynamic transport balance. Liquid leakage was observed at a flow rate higher than 0.6 mL min^{-1}. It is thus suggested that a flow rate of 0.5 mL min^{-1} is optimal.

The performance of two microfluidic DMFCs with normal shaped and ladder-shaped microchannels is shown in Fig. 7. It is obvious that the OCV and the maximum power density of the fuel cell with the ladder-shaped microchannel are higher than those of the DMFC with the normal shaped microchannel. The maximum power density of the microfluidic DMFC with the ladder-shaped microchannel is ca. 35.3% higher than that of a normal shaped microfluidic DMFC. It is believed that the novel design is beneficial in reducing reactant crossover at the liquid-liquid interface, which results in the decrease in the mixed potential, and then leading to a successful increase in both OCV and maximum power density.

5. CONCLUSIONS

The microfluidic DMFC with ladder-shaped microchannel has been proven to be able to obtain better cell performance. The novel ladder-shaped microchannel structure has great effects on reducing the width of mixing zone and hence increasing the reactant transport rate and the fuel utilization to improve the performance of microfluidic DMFC. The highest OCV and maximum power density reach 0.96 V and 12.24 mW cm^{-2}, respectively. The optimization of the parameters for the ladder width should be done to obtain higher performance.

ACKNOWLEDGEMENTS

This work was supported by the National Basic Research Program of China (973 Program) (2012CB932800), the Natural Science Foundation of China (21073219), Shanghai Science and Technology Committee (11DZ1200400) and the Knowledge Innovation Engineering of the CAS (12406, 124091231).

References

1. K.D. Kreuer, *J. Membrane Science*, 185 (2001) 29.
2. J. de Jong, R.G.H. Lammertink, M. Wessling, *Lab on a Chip*, 6 (2006) 1125.
3. E. Kjeang, N. Djilali, D. Sinton, *J. Power Sources*, 186 (2009) 353.
4. S.A. Mousavi Shaegh, N.-T. Nguyen, S.H. Chan, *Int. J. Hydrogen Energy*, (2011) 1.
5. S. F. J. Flipsen, *J. Power Sources*, 162 (2006) 927.
6. R. Ferrigno, A.D. Stroock, T.D. Clark, M. Mayer, G.M. Whitesides, *J. Amer. Chem. Soc.*, 124 (2002) 12930.
7. E. Choban, *J. Power Sources*, 128 (2004) 54.
8. A. Bazylak, D. Sinton, N. Djilali, *J. Power Sources*, 143 (2005) 57.
9. M.-H. Chang, F. Chen, N.-S. Fang, *J. Power Sources*, 159 (2006) 810.

10. P.O. López-Montesinos, N. Yossakda, A. Schmidt, F.R. Brushett, W.E. Pelton, P.J.A. Kenis, *J. Power Sources*, 196 (2011) 4638.
11. G. Miley, N. Luo, J. Mather, E. Byrd, R. Burton, G. Hawkins, R. Gimlin, G. Kopec, P. Shrestha, G. Benavides, J. Laystrom, J. Rusek, T. Valdez, S. Narayanan, *8th Annual International Symposium Small Fuel Cells; Small Fuel Cells for Portable Applications*, Washington, DC, 2006.
12. T.I. Valdez, S.R. Narayanan, *Proceedings of the Electrochemical Society Pennington*, NJ, 2001, pp. 265.
13. M. Sun, G. Velve casquillas, S. Guo, J. Shi, H. Ji, Q. Ouyang, Y. Chen, *Microelectronic Engineering*, 84 (2007) 1182.
14. K. Salloum, J. Hayes, C. Friesen, J. Posner, *J. Power Sources*, 180 (2008) 243.
15. R.F. Ismagilov, A.D. Stroock, P.J.A. Kenis, G. Whitesides, H.A. Stone, *Appl. Phys. Letters*, 76 (2000) 2376.
16. K.V. Sharp, R.J. Adrian, J.G. Santiago, J.I. Molho, *CRC Handbook of MEM*, 2002 6e1.
17. G. Girishkumar, M. Rettker, R. Underhile, D. Binz, K. Vinodgopal, P. McGinn, P. Kamat, *Langmuir*, 21 (2005) 8487.
18. D.C. Duffy, J.C. McDonald, O.J.A. Schueller, G.M. Whitesides, *Anal. Chem.*, 70 (1998) 4974.
19. Y. Song, C. Batista, R. Sarpeshkar, J. Han, *J. Power Sources*, 183 (2008) 674.
20. X. Wang, W. Li, Z. Chen, M. Waje, Y. Yan, *J. Power Sources*, 158 (2006) 154.
21. N.V. Zaytseva, V.N. Goral, R.A. Montagna, A.J. Baeumner, *Lab on a Chip*, 5 (2005) 805